Relative acoustic impedance from wavelet transform

Marcílio Castro de Matos[1], Rodrigo Penna[2], Paulo Johann[2], and Kurt Marfurt[3]

Abstract

Most deconvolution algorithms try to transform the seismic wavelet into spikes by designing inverse filters that remove an estimated seismic wavelet from seismic data. We assume that seismic trace subtle discontinuities are associated with acoustic impedance contrasts and can be characterized by wavelet transform spectral ridges, also called modulus maxima lines (WTMML), allowing us to improve seismic resolution by using the wavelet transform. Specifically, we apply the complex Morlet continuous wavelet transform (CWT) to each seismic trace and compute the WTMMLs. Then, we reconstruct the seismic trace with the inverse continuous wavelet transform from the computed WTMMLs with a broader band complex Morlet wavelet than that used in the forward CWT. Because the reconstruction process preserves amplitude and phase along different scales, or frequencies, the result looks like a deconvolution method. Considering this high-resolution seismic representation as a reflectivity approximation, we estimate the relative acoustic impedance (RAI) by filtering and trace integrating it. Conventional deconvolution algorithms assume the seismic wavelet to be stochastic, while the CWT is implicitly time varying such that it can be applied to both depth and time-domain data. Using synthetic and real seismic data, we evaluated the effectiveness of the methodology on detecting seismic events associated with acoustic impedance changes. In the real data examples, time and in-depth RAI results, show good correlation with real P-impedance band-pass data computed using more rigorous commercial inversion software packages that require well logs and low-frequency velocity model information.

Introduction

Deconvolution of separate earth reflectivity from the seismic wavelet is still an important research topic. Deconvolution increases temporal resolution and yields a representation of subsurface reflectivity by compressing the basic seismic wavelet in the seismogram (Yilmaz, 2001). Most existing deconvolution algorithms involve first estimating the seismic wavelet and then designing an inverse filter to remove these wavelets from the seismic trace (Lines and Ulrych, 1977). These algorithms also assume that seismic traces can be modeled by convolving a basic seismic wavelet with the earth reflectivity (Yilmaz, 2001).

Nowadays, joint time-frequency filtering methods, such as the wavelet transform, are widely used to filter undesired noise such as ground roll and air waves (de Matos and Osório, 2002). Filtering is implemented by exploiting the high redundancy of the joint time-frequency representation that, ideally, maps the noise and signal to different regions of the time-frequency plane. The processor identifies the noise component of the data, mutes or otherwise attenuates it, and reconstructs the signal from the remaining components. Among several joint time-frequency techniques, the continuous wavelet transform (CWT) is widely used and can be interpreted as a lookup tool that enhances certain signal features at different scales or frequencies. Using wavelet transform ridges detected along the scales, called the modulus maxima lines (WTMMLs), Herrmann and Stark (2000), de Matos et al. (2007), and Li and Liner (2008) show how to characterize seismic trace subtle discontinuities and how they can be associated with acoustic impedance contrasts.

Therefore, because the WTMML can be associated with earth reflectivity, we propose a CWT filtering algorithm that reinforces the acoustic impedance contrasts by compressing the inverse continuous wavelet transform (ICWT) wavelet.

We begin our paper by reviewing WTMML theory and showing how it can be associated with seismic singularities. Next, we present how the WTMML can be used to reconstruct a high-resolution seismic trace through

[1]SISMO Research & Consulting, Rio de Janeiro, Brazil and The University of Oklahoma, Norman, Oklahoma, USA. E-mail: marcilio@matos.eng.br.
[2]Petrobras, Rio de Janeiro, Brazil. E-mail: rpenna@petrobras.com.br; johann@petrobras.com.br.
[3]The University of Oklahoma, Norman, Oklahoma, USA. E-mail: kmarfurt@ou.edu.

Manuscript received by the Editor 15 June 2013; revised manuscript received 18 September 2013; published online 31 January 2014. This paper appears in *Interpretation*, Vol. 2, No. 1 (February 2014); p. SA107–SA118, 21 FIGS.
http://dx.doi.org/10.1190/INT-2013-0090.1. © 2014 Society of Exploration Geophysicists and American Association of Petroleum Geologists. All rights reserved.

Downloaded 02/10/14 to 129.15.127.245. Redistribution subject to SEG license or copyright; see Terms of Use at http://library.seg.org/

ICWT and the relative acoustic impedance (RAI) attribute from the high-resolution seismic trace. Finally, we show how seismic interpretation can be improved by applying the proposed methodology to both synthetic and real seismic data.

ICWT Deconvolution–iCWTdec

The CWT is formalized by Grossman and Morlet (1984) and is defined as the crosscorrelation between a signal, i.e., the seismic trace, and the enlarged and compressed versions of a basic wavelet (or "mother") function having zero mean, at different scales. The CWT can also be interpreted as the convolution between the seismic trace and the same (but time reversed) basic scaled wavelets. In this manner, we can interpret the CWT as a band-pass filter bank, and consequently, we can state that the CWT is a time-frequency or spectral decomposition method.

After CWT, each seismic trace is transformed into a time (or depth)-versus-scale (or frequency bandwidth) matrix. Each matrix coefficient represents how well the seismic trace correlates to each dilated wavelet as a function of time (or depth).

Mallat and Zhong (1992) show how the CWT can be used to detect multiscale edges by identifying modulus maxima lines (WTMML) along the scales. Tu and Hwang (2005) extend the same concept to complex wavelets. The manner in which the WTMML varies along the scales determines the sharpness of the edges. Specifically, a parameter called the Lipschitz, or Holder exponent, is calculated by taking the derivative of the WTMML using a logarithmic scale. Borrowing hints found in Mallat and Zhong (1992), Herrmann and Stark (2000), and Li and Liner (2008) show that the Lipschitz coefficients can be used to characterize acoustic impedance contrasts when applied to seismic data with appropriate wavelet functions, while de Matos et al. (2007) use the whole WTMML to cluster different seismic facies.

Mallat and Zhong (1992) also show that the original signal can be approximately reconstructed using a multiscale edge representation. In fact, the seismic trace can be reconstructed from its CWT coefficients by integrating over time and frequency the coefficients multiplied by each dilated basic wavelet (Teolis, 1998). If a perfect trace reconstruction is not required, then any wavelet function can be used with the ICWT.

Assuming that the WTMML is associated with important acoustic impedance contrasts, we propose in this paper to reconstruct each seismic trace directly from the detected WTMMLs using a shrunken complex Morlet wavelet rather than the Morlet wavelet used in the forward CWT decomposition of the seismic data. In this manner, despite the different analysis and synthesis wavelet used, the CWT magnitude and phase are preserved and the ICWT reconstruction simply removes the wavelet side lobe effects of the main seismic events.

The proposed methodology is summarized as follows:

1) Compute the complex Morlet CWT of each seismic trace.
2) From the CWT magnitude, extract the WTMMLs that fall above an interpreter-defined threshold.
3) Compute the ICWT from WTMML coefficients using a shrunken Morlet wavelet.
4) Compute the RAI by band-pass integrating (Berteussen and Ursin, 1983) the ICWT.

Formally, deconvolution algorithms require a stochastic wavelet, which often occurs for time-domain data where one can use the convolutional model to synthesize the seismic data from the earth reflectivity. Because of lateral and vertical velocity variations, the seismic wavelet is no longer stochastic. Unlike deconvolution, the proposed algorithm enhances the seismic resolution of stochastic data and thus works equally well in the time and depth domains. Because the proposed workflow mimics a deconvolution process, we owe it the name iCWTdec.

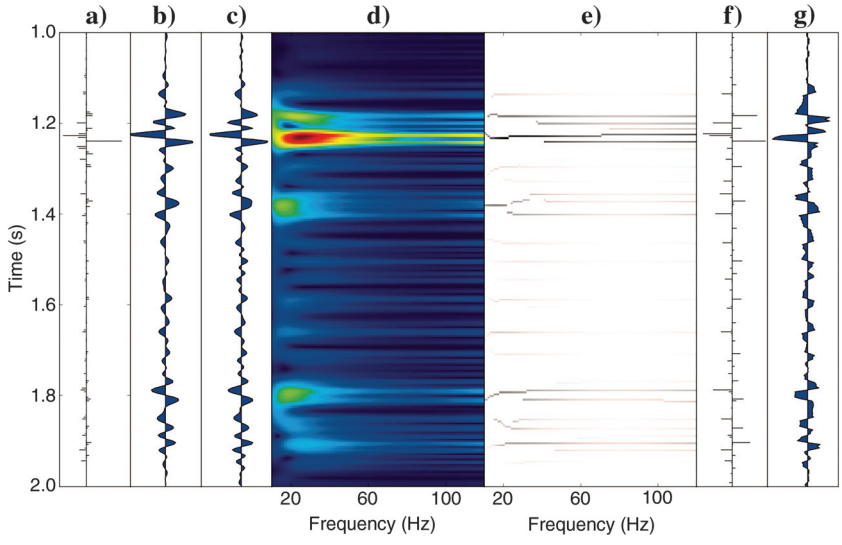

Figure 1. Panel (a) shows a 4 ms sampled real reflectivity series. (b) Synthetic trace obtained by convolving (a) with a 30 Hz Ricker wavelet. (c) Closest seismic trace to the correspondent well: (d) its Morlet CWT magnitude and (e) spectral ridges (WTMML); (f) iCWTdec trace and (g) RAI from iCWTdec.

Downloaded 02/10/14 to 129.15.127.245. Redistribution subject to SEG license or copyright; see Terms of Use at http://library.seg.org/

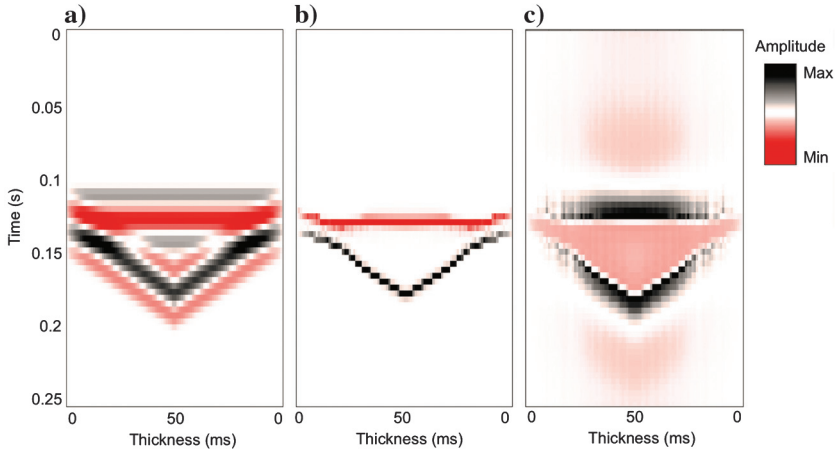

Figure 2. (a) Synthetic channel model, (b) its corresponding ICWT deconvolution, and (c) the RAI.

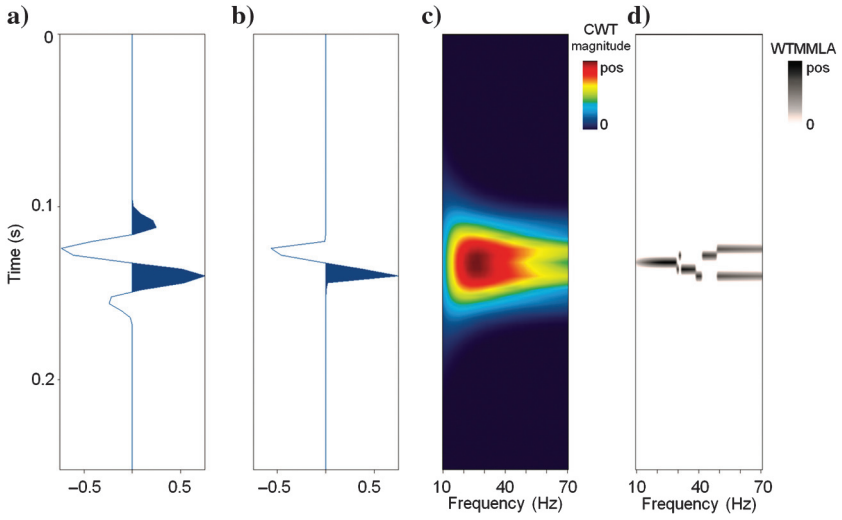

Figure 3. Plot (a) shows 10 ms thickness trace, (b) ICWT deconvolution trace, (c) CWT Morlet magnitude, and (d) CWT modulus maxima.

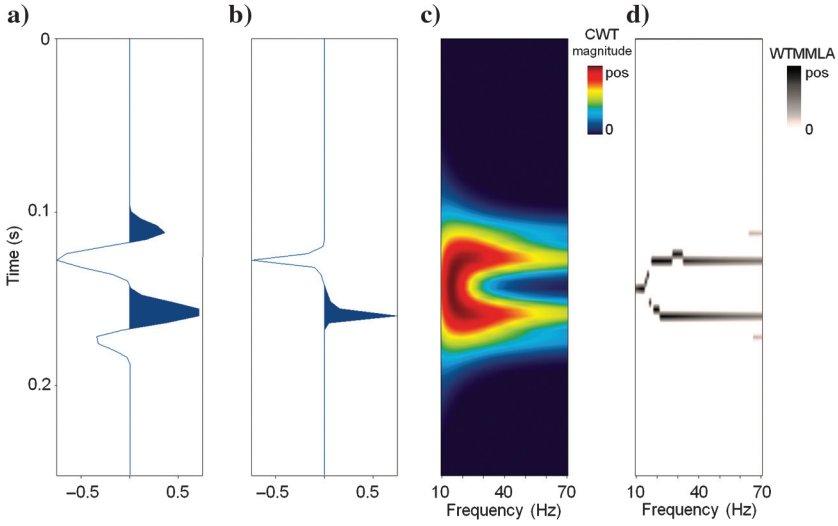

Figure 4. Plot (a) shows 30 ms thickness trace, (b) ICWT deconvolution trace, (c) CWT Morlet magnitude, and (d) CWT modulus maxima.

Downloaded 02/10/14 to 129.15.127.245. Redistribution subject to SEG license or copyright; see Terms of Use at http://library.seg.org/

Downloaded 02/10/14 to 129.15.127.245. Redistribution subject to SEG license or copyright; see Terms of Use at http://library.seg.org/

Figure 1 illustrates schematically how the proposed algorithm works using a real seismic trace. First, we generate the reflectivity series 4 ms sampled (Figure 1a), from real well log data. Comparing the 30 Hz Ricker wavelet filtered synthetic seismic (Figure 1b) and the closest seismic trace (Figure 1c), we can confirm a good well tie. The Morlet CWT (Figure 1d) of the seismic is computed, and the ridges of the CWT magnitude along the scales are detected (Figure 1e) and used as a guide to reconstruct the higher resolution trace using a shrunken Morlet wavelet (Figure 1f). Finally, after band-pass integration, the RAI is computed (Figure 1g).

We shall illustrate the use of such a workflow by using synthetic and real data examples.

Example 1: Synthetic seismic channel

To test the proposed methodology, we first apply it to a 2D synthetic seismic response of a channel with thickness varying from 1 to 50 ms convolved with a band-pass wavelet (Figure 2a).

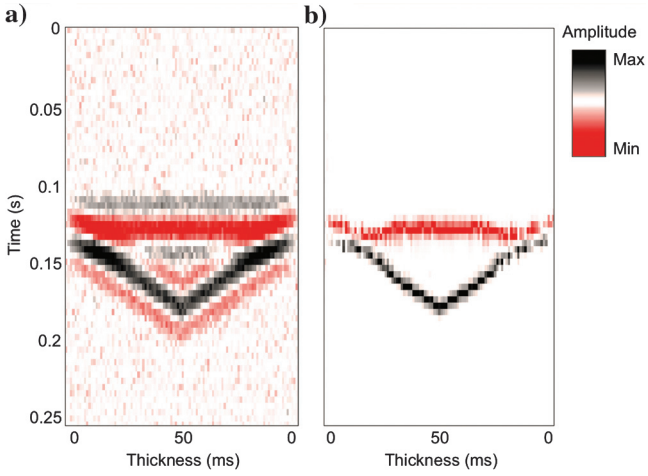

Figure 5. (a) Noisy channel model and (b) corresponding ICWT deconvolution.

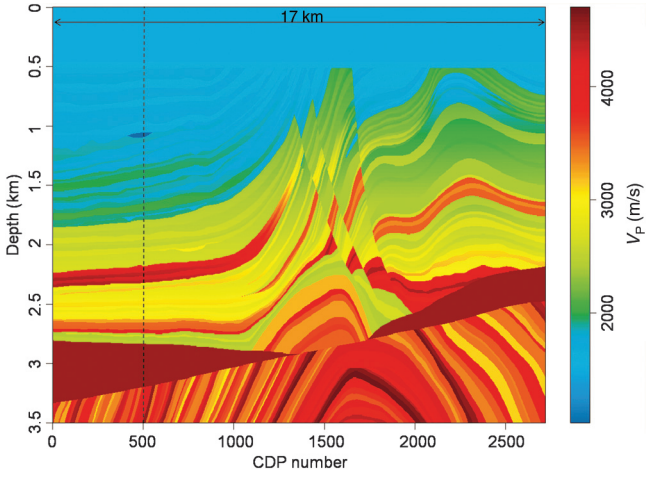

Figure 6. Marmousi2 V_P model (Martin, 2004).

Figures 3a and 4a show the synthetic traces at 10 and 30 ms thickness. Figures 3b and 4b show the corresponding ICWT-reconstructed traces. Figures 3c and 4c show the Morlet CWT magnitudes, which, associated with Figures 3d and 4d, show the desired seismic events after the WTMML detection.

Applying this process to all the traces in Figure 2a, we obtain the iCWTdec image in Figure 2b. Note the improvement in the temporal resolution of the proposed methodology.

By integrating the reflectivity series, we also calculated the RAI. Figure 2c shows the RAI.

Figure 5 shows how the proposed algorithm also works well after applying random additive noise to the same synthetic data.

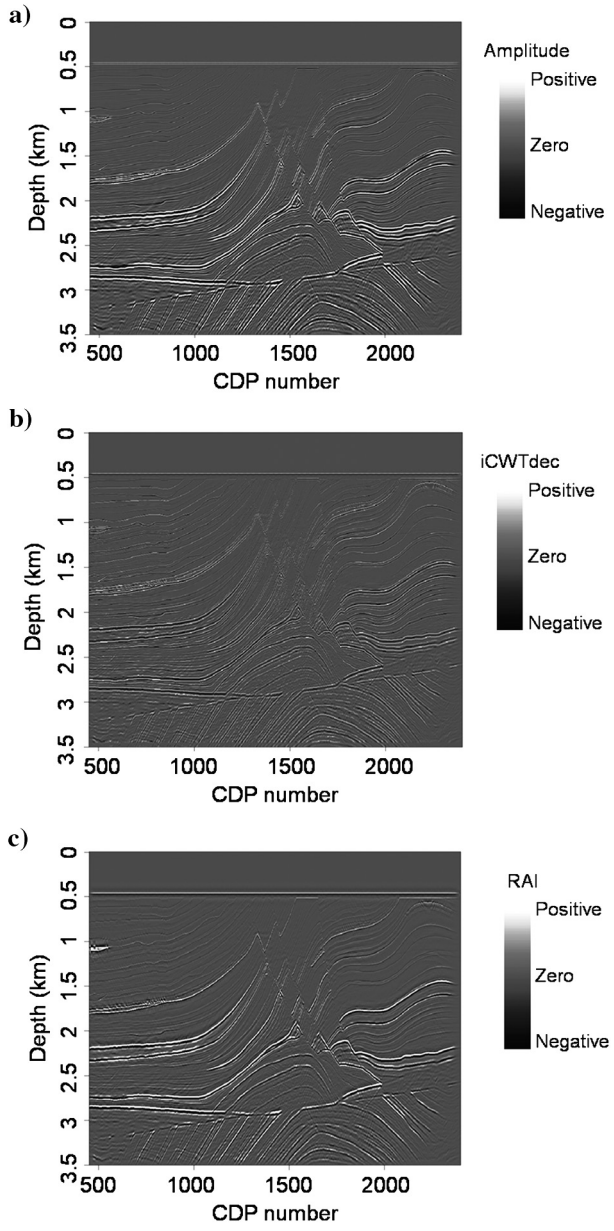

Figure 7. (a) Wave equation prestack depth migrated synthetic seismic section from Marmousi2 model, (b) iCWTdec, and (c) RAI.

Example 2: Marmousi2 synthetic data

Figure 6 shows the Marmousi2 V_P model. This model is designed by Martin (2004) to evaluate AVO attributes after different seismic processing schemes. Different from our simple convolutional first example, Martin (2004) uses elastic wave-equation forward modeling to keep realistic seismic events, such as multiples, head waves, etc. In this paper, we used Martin's (2004) wave-equation prestack depth-migrated data set (Figure 7a) to test our proposed algorithm.

Although the data in Figure 7a are in depth, we can further enhance vertical resolution directly applying the iCWTdec. Figure 7b shows the iCWTdec, while Figure 7c displays the band-pass integration result, or RAI, computed from the iCWTdec data.

Figure 8a shows a representative trace from the V_P section shown in Figure 6 indicated by a vertical dotted line. Figure 8a shows the migrated trace, and Figure 8c shows the ICWT deconvolved trace. Note the improvement in resolution even though the wavefield is not stochastic.

Example 3: Real data offshore Brazil in time

The depositional model of our Campos Basin turbidite reservoirs data example is as a complex turbidity system, mainly represented by amalgamated channels, lobes and overbank facies (Bruhn et al., 2003). The heterogeneities related to the erosive channels and small displacement faults fall below seismic resolution and are therefore tough to detect. The traps are

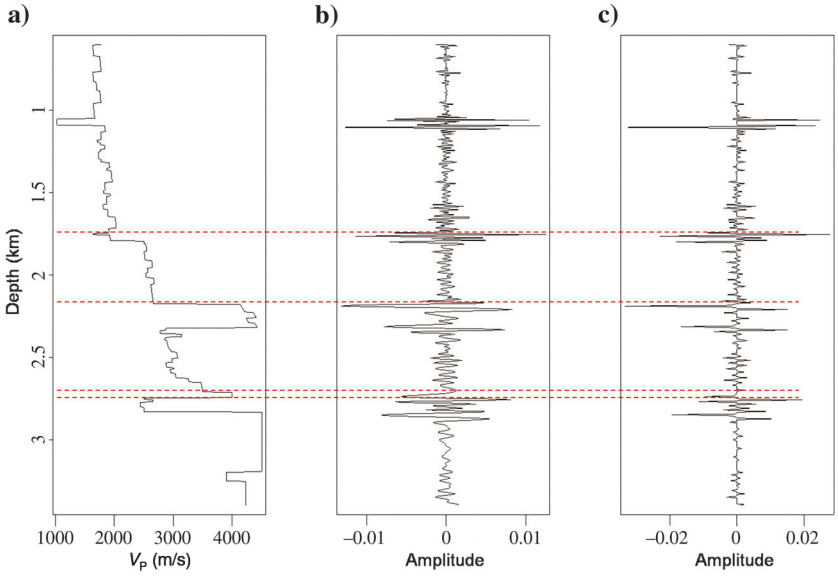

Figure 8. (a) The V_P trace at CDP 500 from Figure 8. (b) Seismic trace at CDP 500 from Figure 7a. (c) ICWT deconvolved data trace at CDP 500 from Figure 7b.

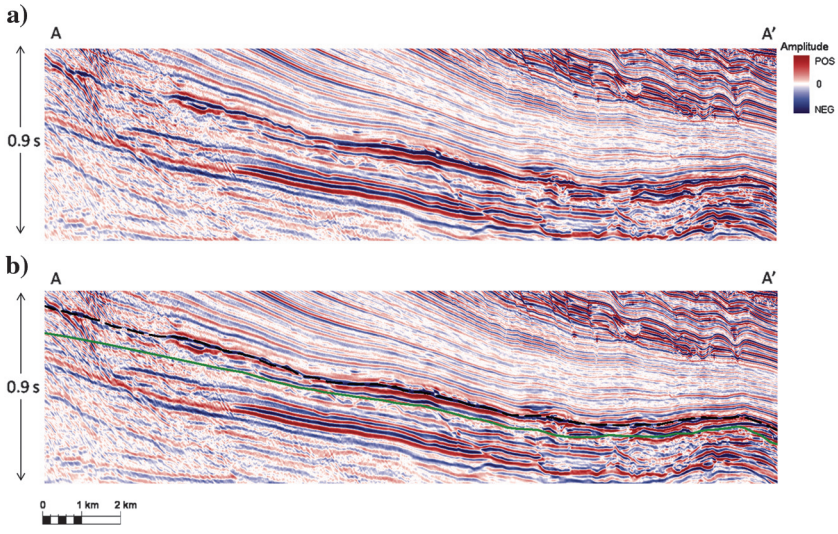

Figure 9. (a) Vertical seismic line AA′. (b) The black dashed line shows the top horizon of the upper reservoir zone, and the green line shows the bottom horizon of the base reservoir zone.

Downloaded 02/10/14 to 129.15.127.245. Redistribution subject to SEG license or copyright; see Terms of Use at http://library.seg.org/

essentially stratigraphic, with some secondary structural components (Lemos et al., 2006).

Figure 9a shows a representative vertical slice through the 3D seismic amplitude data. The dashed black line in Figure 9b indicates the top of the upper reservoir zone, and the green line shows the bottom of the lower reservoir zone. Figure 10 shows the map of the root-mean-square (rms) amplitude value between top and base of the upper reservoir zone, where one can see the complex-channel turbidite sedimentary system and also the deposition direction and amalgamated stack.

After applying the proposed methodology to the whole 3D seismic data, Figure 11a and 11b illustrates the same line shown in Figure 9 of the iCWTdec and RAI attributes, respectively. The iCWTdec results clearly help to better discriminate the limits of the main stratigraphic sequences.

Using a commercial sparse-spike model-based acoustic inversion (Levy and Fullagar, 1981) software assisted by well logs, we computed the P-impedance, and we applied a low-cut filter to generate a P-impedance band-pass attribute, here shown in Figure 11c. By visually comparing Figure 11b and 11c, we see that RAI is a reasonable approximation to band-limited P-impedance. In addition, iCWTdec (Figure 11a) explicitly shows the location of the impedance changes.

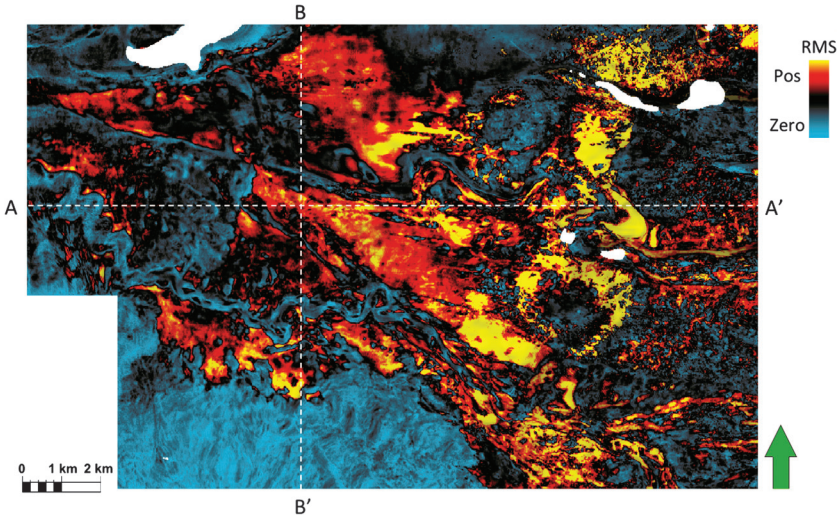

Figure 10. Horizon slice through the rms seismic amplitude values around the top of the upper reservoir zone. AA′ and BB′ indicate the vertical lines' locations.

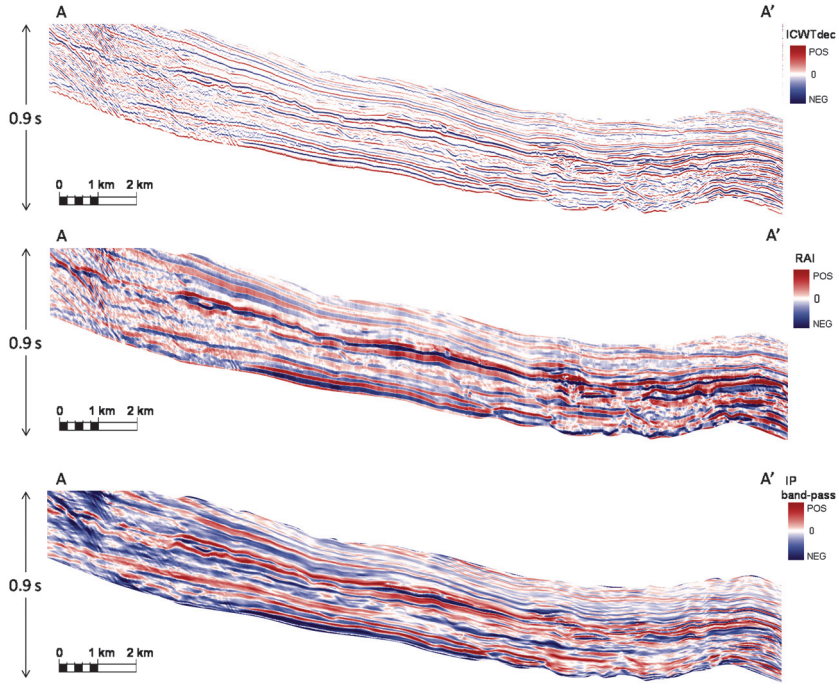

Figure 11. (a) The iCWTdec vertical slices AA′, (b) RAI, and (c) P-impedance band-pass.

Downloaded 02/10/14 to 129.15.127.245. Redistribution subject to SEG license or copyright; see Terms of Use at http://library.seg.org/

Downloaded 02/10/14 to 129.15.127.245. Redistribution subject to SEG license or copyright; see Terms of Use at http://library.seg.org/

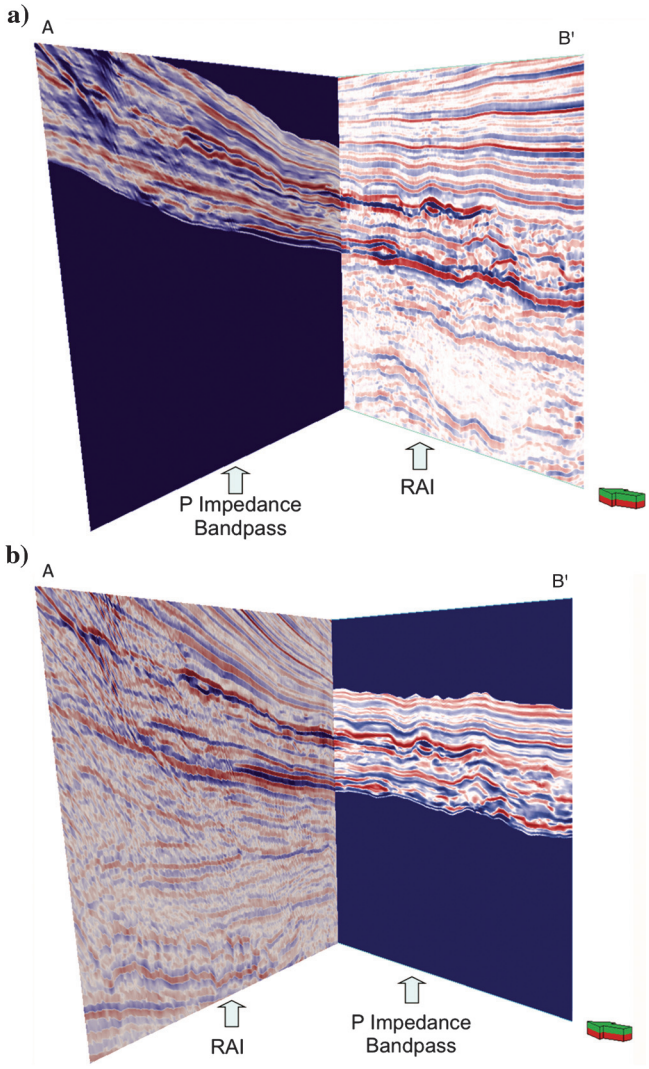

Figure 12. (a) The 3D visualization of the AA′ P-impedance band-pass and BB′ RAI vertical lines, respectively, and conversely (b) AA′ RAI and BB′ P-impedance band-pass RAI vertical lines, respectively.

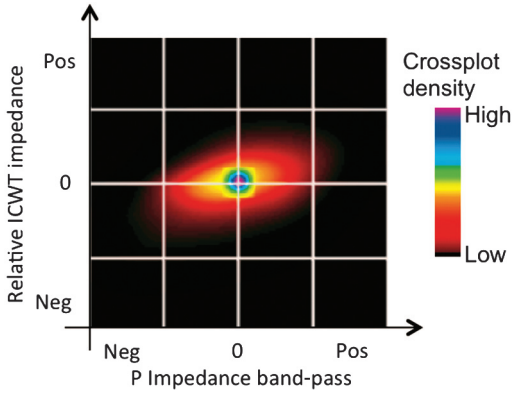

Figure 13. RAI × P-impedance band-pass crossplot values around the top of the upper reservoir zone.

Figure 12 uses 3D visualization to compare two workflows by sliding a RAI crossline over the P-impedance band-pass inline, and vice versa. Note the continuity at the intersection neighborhood when changing from one attribute to another.

In Figure 13, we try to be quantitative by crossplotting RAI and P-impedance band-pass values between the top of the upper reservoir zone to the bottom of the lower level reservoir zone, and the fairly linear result gives us some confidence to use RAI as a band-pass impedance estimation, when few, limited, or no well log data are available.

As a final visual comparison, Figure 14a displays the horizon slice of the rms RAI values between the top and base of the upper reservoir zone, and Figure 14b shows the P impedance band-pass obtained by model-based inversion rms values for the same time interval. Once again, the turbidite-like depositional system shown previously in Figure 10 is very similar in both slices.

Example 4: Real data offshore Brazil in depth

This real 3D seismic data are depth migrated, sampled in depth, and also come from the Campos Basin, Brazil. Figure 15a shows a vertical user-defined section through the seismic amplitude volume. The maximum amplitude between closest top horizon zero crossings horizon slice is illustrated in Figure 16. The top and base of the target region are shown in Figure 15b.

Although the data are sampled in depth, we apply iCWTdec and RAI and compute the high-resolution seismic trace (Figure 17a) and the band-pass integration of the high-resolution trace (Figure 17b).

Because the 3D seismic data are in depth, the following model-based acoustic inversion workflow should be applied to the seismic data in time. We must first (1) convert seismic data from depth to time using a velocity model, then (2) compute the model-based P-impedance band-pass and finally, (3) convert the inversion results back from time to depth. Figure 18 compares the workflow for the RAI algorithm and the band-passed model based inversion. Figure 17c shows the P-impedance band-pass section.

Using 3D visualization, Figure 19 shows an RAI crossline over the P-impedance band-pass inline, and vice versa. In this manner, we can check the continuity of the intersection neighborhood when we change from one attribute to another.

The crossplot between RAI and P-impedance band-pass values around the top horizon (Figure 20) confirms a linear trend linking both attributes. The rms value maps using the same time window are plotted in Figure 21a and 21b for the RAI and P-impedance band-pass, respectively. Note how anomalies, structural features, and facies associations are equal for both maps.

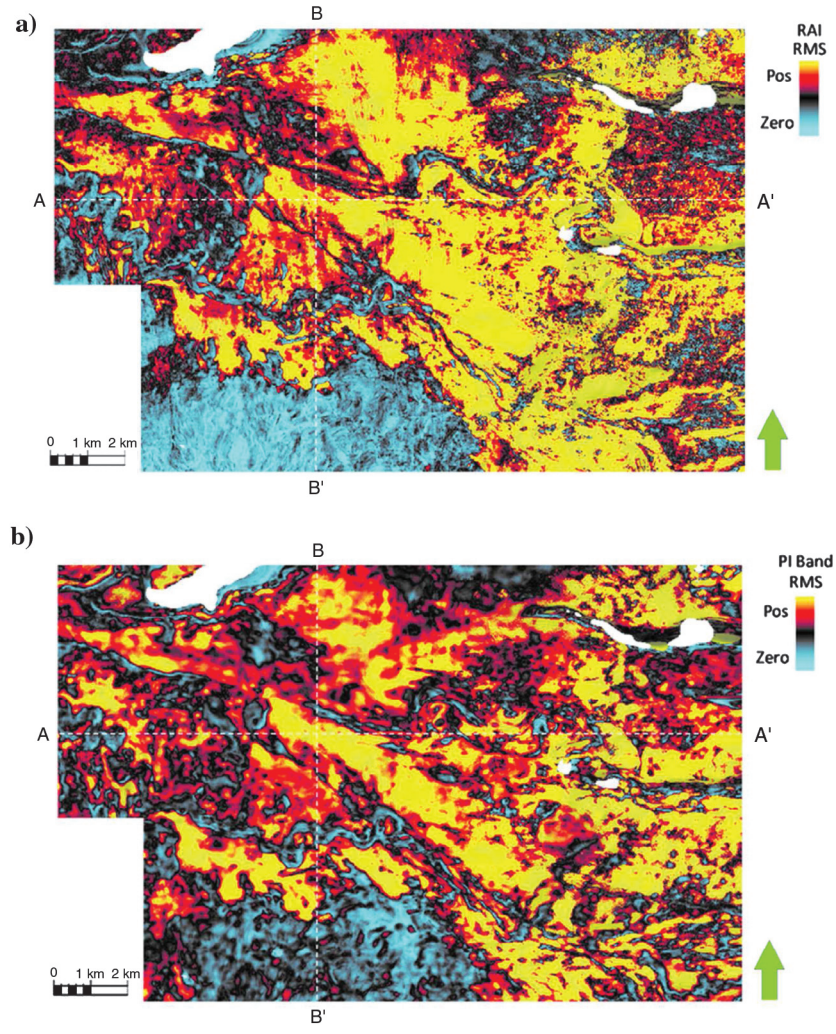

Figure 14. (a) RAI and (b) P-impedance band-pass horizon map of the rms values around the top of the upper reservoir zone.

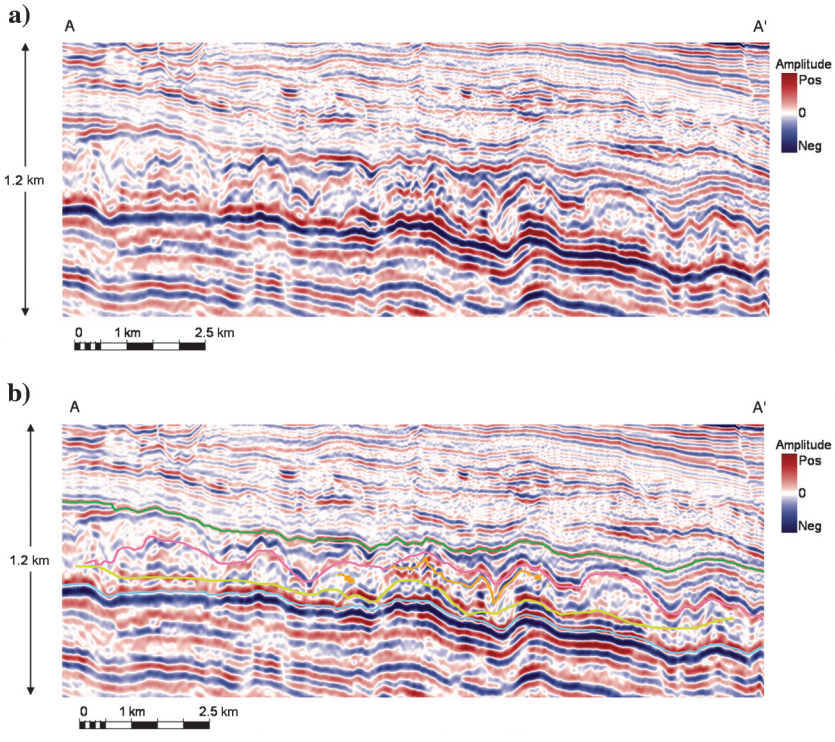

Figure 15. (a) Vertical seismic line AA′ and (b) the equivalent interpreted line.

Downloaded 02/10/14 to 129.15.127.245. Redistribution subject to SEG license or copyright; see Terms of Use at http://library.seg.org/

Conclusions

The CWT spectral decomposition filtering process described generates high-resolution events that correlate to major acoustic impedance changes. Such higher-resolution images can be particularly valuable in resolving thin beds approaching the limits of seismic resolution. Because this frequency broadening is a trace-by-trace independent process, laterally consistent thin-bed terminations and other truncations can be interpreted with confidence. As a seismic resolution enhancement algorithm, iCWTdec can be applied directly to data in depth.

Comparisons between RAI and more time- and data-intensive P-impedance band-pass computed from

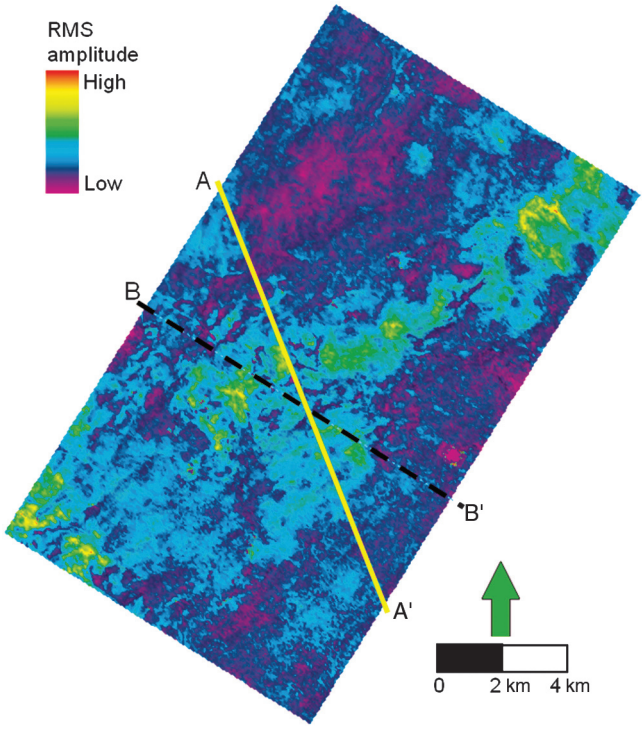

Figure 16. Horizon map of the maximum seismic amplitude between zero crossings around the upper horizon.

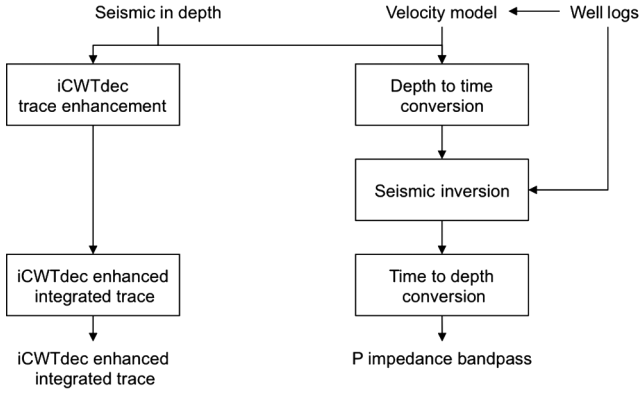

Figure 18. Acoustic inversion workflow applied to seismic data sampled in depth compared with the RAI.

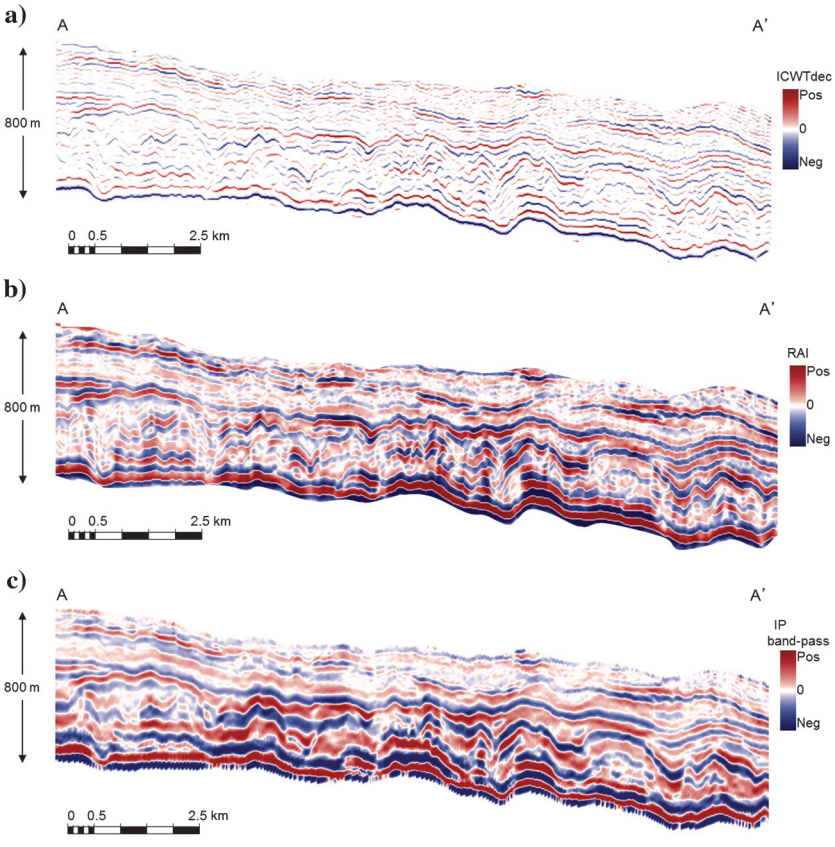

Figure 17. (a) The iCWTdec vertical slices AA′, (b) RAI, and (c) P-impedance band-pass.

Downloaded 02/10/14 to 129.15.127.245. Redistribution subject to SEG license or copyright; see Terms of Use at http://library.seg.org/

acoustic inversion algorithms are good, suggesting that we can use RAI, mainly, for explorationist purposes, when few or no wells are available.

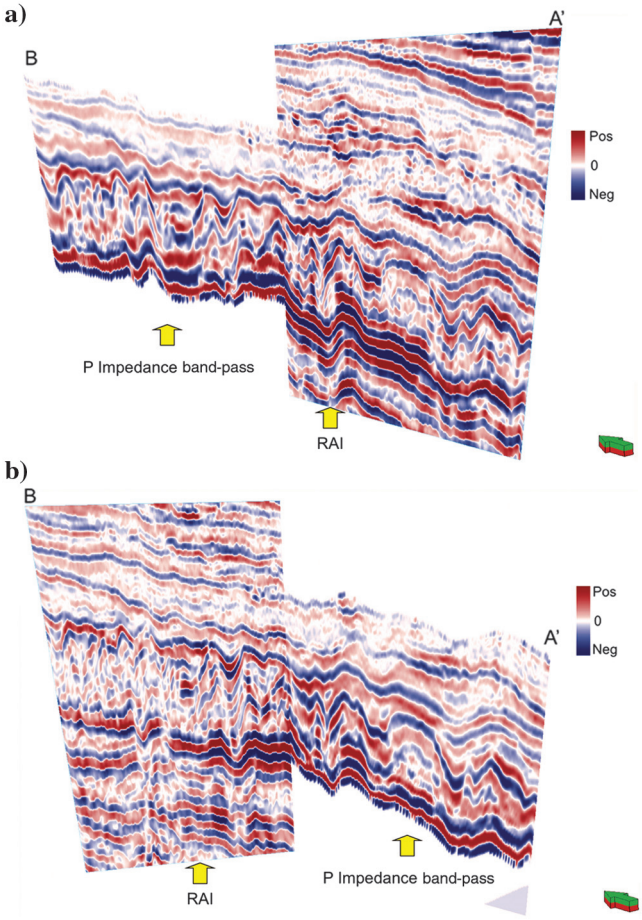

Figure 19. (a) The 3D visualization of AA′ P-impedance band-pass and BB′ RAI vertical lines, respectively, and conversely (b) AA′ RAI and BB′ P-impedance band-pass RAI vertical lines, respectively.

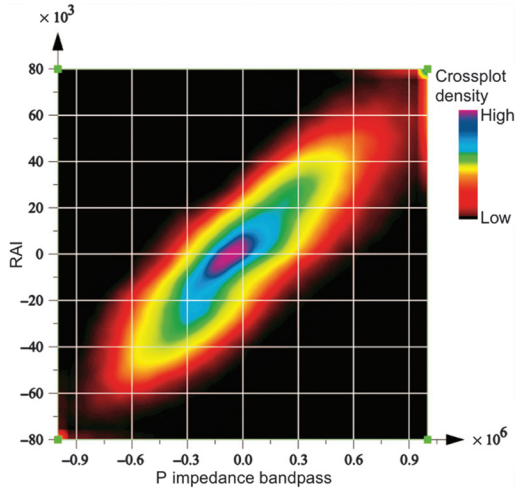

Figure 20. RAI × P-impedance band-pass crossplot values around the top of the upper reservoir zone.

The spectrum of the forward complex Morlet wavelet should accurately express (and if desired, reconstruct) the bandwidth of the input traces. The

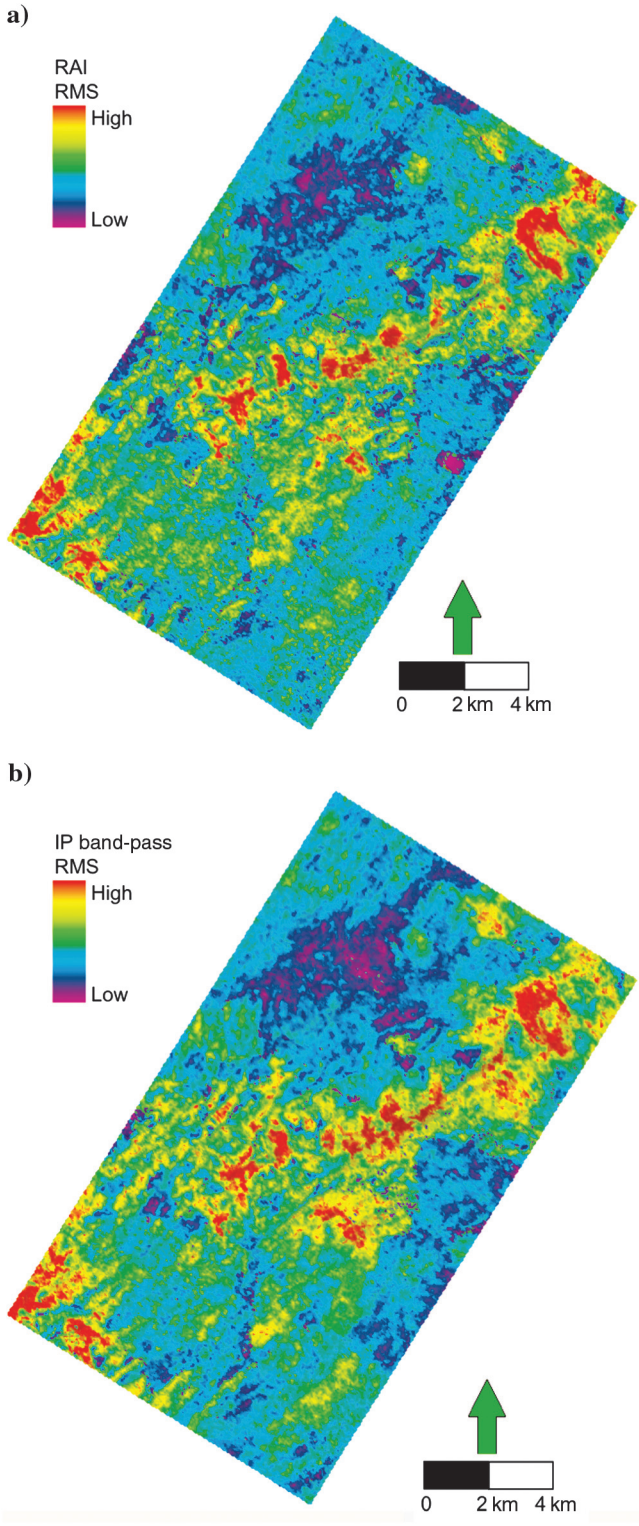

Figure 21. (a) RAI and (b) P-impedance band-pass horizon map of the rms values around the top of the upper reservoir zone.

Downloaded 02/10/14 to 129.15.127.245. Redistribution subject to SEG license or copyright; see Terms of Use at http://library.seg.org/

CWT magnitude and the WTMML analysis of representative vertical slices should be examined to confirm if the chosen scales (frequency band) and thresholds used to detect WTMML anomalies detect and delineate the features of interest.

In this paper, we reconstruct the seismic trace by preserving all the WTMML scales, giving rise to a broadband reconstruction.

Acknowledgments

The authors would like to thank Petrobras for providing the license to publish and use the real data. The first and fourth authors also would like to thank the industry sponsors of the University of Oklahoma Attribute-Assisted Seismic Processing and Interpretation (AASPI) Consortium.

References

Berteussen, K. A., and B. Ursin, 1983, Approximate computation of the acoustic impedance from seismic data: Geophysics, **48**, 1351–1358, doi: 10.1190/1.1441415.

Bruhn, C. H. L., J. A. T. Gome, C. D. Lucchese, Jr, and P. R. S. Johann, 2003, Campos Basin: Reservoir characterization and management — Historical overview and future challenges: Presented at Offshore Technology Conference.

de Matos, M. C., and P. L. M. Osório, 2002, Wavelet transform filtering in the 1D and 2D for ground roll suppression: 72nd Annual International Meeting, SEG, Expanded Abstracts, 2245–2248.

de Matos, M. C., P. L. M. Osório, and P. R. S. Johann, 2007, Unsupervised seismic facies analysis using wavelet transform and self-organizing maps: Geophysics, **72**, no. 1, P9–P21, doi: 10.1190/1.2392789.

Grossmann, A., and J. Morlet, 1984, Decomposition of Hardy functions into square integrable wavelets of constant shape: SIAM Journal on Mathematical Analysis, **15**, 723–736, doi: 10.1137/0515056.

Herrmann, F., and C. Stark, 2000, A scale attribute for texture in well and seismic data: 70th Annual International Meeting, SEG, Expanded Abstracts, 2063–2066.

Lemos, W. P., M. R. B. Castro, C. M. Soares, J. F. Rosalba, and A. A. G. Meira, 2006, Albacora Leste Field development: Reservoir aspects and development strategy: Presented at Offshore Technology Conference.

Levy, S., and P. K. Fullagar, 1981, Reconstruction of a sparse spike train from a portion of its spectrum and application to high-resolution deconvolution: Geophysics, **46**, 1235–1243, doi: 10.1190/1.1441261.

Li, C., and C. Liner, 2008, Wavelet-based detection of singularities in acoustic impedances from surface seismic reflection data: Geophysics, **73**, no. 1, V1–V9, doi: 10.1190/1.2795396.

Lines, L. R., and T. J. Ulrych, 1977, The old and the new in seismic deconvolution and wavelet estimation: Geophysical Prospecting, **25**, 512–540, doi: 10.1111/j.1365-2478.1977.tb01185.x.

Mallat, S., and S. Zhong, 1992, Characterization of signals from multiscale edges: IEEE Transactions on Pattern Analysis and Machine Intelligence, **14**, 710–732, doi: 10.1109/34.142909.

Martin, G., 2004, The Marmousi2 model, elastic synthetic data, and an analysis of imaging and AVO in a structurally complex environment: M.S. thesis, University of Houston.

Teolis, A., 1998, Computational signal processing with wavelets, 1st ed.: Birkhäuser.

Tu, C. L., and W. L. Hwang, 2005, Analysis of singularities from modulus maxima of complex wavelets: IEEE Transactions on Information Theory, **51**, 1049–1062, doi: 10.1109/TIT.2004.842706.

Yilmaz, Ö., 2001, Seismic data analysis: SEG.

Marcílio Castro de Matos received a B.S. (1988) and an M.S. (1994) in electrical engineering from the Instituto Militar de Engenharia (IME) and a doctoral degree (2004) from the Pontificia Universidade Catolica do Rio de Janeiro. He served from 1989 to 1999 as a military engineer at the Brazilian Army Test Center and at IME as a signal processing military professor from 1999 to 2010. He was a visiting scholar at the University of Oklahoma from January 2008 to January 2010. He is currently coinvestigator of the Attribute-Assisted Seismic Processing & Interpretation Research Consortium at the University of Oklahoma and is the principal of SISMO Signal Processing Research, Training & Consulting. His research interests include applied seismic analysis, digital signal processing, spectral decomposition, and seismic pattern recognition.

Rodrigo Penna received a bachelor's (2006) degree in geology from the Federal University of Minas Gerais. He has been working at Petrobras as a reservoir geophysicist since 2008, working with seismic inversion, 3D interpretation, and structural attributes generation.

Paulo Johann received a degree (1980) in geology from the Vale do Rio dos Sinos University, a Master's degree (1994) and a doctorate (1997) from the Paris VI University. He is currently the reservoir geophysics manager for Petrobras, based in Rio de Janeiro. He previously served as vice-president of both the Brazilian Geophysical Society and SEG, and in 2008 became the first Central & South America regional SEG distinguished lecturer.

Downloaded 02/10/14 to 129.15.127.245. Redistribution subject to SEG license or copyright; see Terms of Use at http://library.seg.org/

Kurt J. Marfurt joined the University of Oklahoma in 2007, where he serves as the Frank and Henrietta Schultz Professor of Geophysics within the ConocoPhillips School of Geology and Geophysics. His primary research interests include the development and calibration of new seismic attributes to aid in seismic processing, seismic interpretation, and reservoir characterization. His recent work has focused on correlating seismic attributes such as volumetric curvature, impedance inversion, and azimuthal anisotropy with image logs and microseismic measurements with a particular focus on resource plays. In addition to teaching and research duties at the University of Oklahoma, he leads short courses on attributes for SEG and AAPG.

Downloaded 02/10/14 to 129.15.127.245. Redistribution subject to SEG license or copyright; see Terms of Use at http://library.seg.org/